J Nanostruct 16(4): 5107-5120, Autumn 2026

RESEARCH PAPER

Enhanced OLED Performance via Graphene Oxide Nanocomposite-Modified PEDOT:PSS as a Hole Injection Layer

Shurooq S. Mahmood

Department of Physics, College of Education, Al-Iraqia University, Baghdad, Iraq

ARTICLE INFO

Article History:
Received 06 April 2026
Accepted 20 June 2026
Published 01 October 2026

Keywords:
Graphene oxide
Hole Injection Layer
Nanocomposite
Organic Light-Emitting Diodes
PEDOT: PSS

ABSTRACT

Organic Light Emitting Diodes (OLEDs) have emerged as one of the most promising technologies for display and solid-state lighting applications, but they are limited in both operational lifetime and performance by their respective hole injection layer (HIL). Poly(3,4-ethylenedioxythiophene): polystyrene sulfonate (PEDOT:PSS) is currently the most widely used solution processed HIL; however, its limitations, such as acidification-induced indium tin oxide (ITO) corrosion and insufficient work function (~5.1 eV) and moderate conductivity prohibit the creation of long-lived, high-performance devices. We present findings that Graphene Oxide (GO) can be utilized as an effective nanofiller within PEDOT: PSS to enhance its performance as the HIL for red phosphorescent OLEDs. Graphene Oxide (GO) was synthesized using a modified Hummers' method and incorporated into PEDOT: PSS at different weight loadings (0.25 to 2.0 wt %). The optimum GO weight loading was determined to be 0.5 wt % which resulted in a dramatic increase (36-fold) in conductivity (33.3 S/cm), increased work function by 0.25 eV (to 5.35 eV) and reduced surface roughness to 1.18 nm. Electrical measurements showed that rigid OLEDs fabricated using the optimized HIL from PEDOT: PSS/GO composite had a turn-on voltage of 2.5 V, maximum luminance of 48,300 cd/m^2, peak current efficiency of 21.9 cd/A and peak external quantum efficiency of 18.4%. One of the most notable results was the four-fold increase in operational half-lifetime (T50) from 35 h to 142 h at 25 mA/cm^2 operational current. Post-mortem analysis of the devices again showed that GO leads to suppression of ITO corrosion and indium ion migration via hydrogen bonding passivation of acid groups within the PSS matrix, and also acts as a barrier nanofiller to prevent moisture and oxygen ingress. Additionally, the composite HIL is mechanically stable on graphene-anode substrates with 91% of the luminance retained after 1000 bending cycles. This work establishes GO/PEDOT: PSS nanocomposites as a scalable, multifunctional hole injection platform that simultaneously enhances efficiency, stability, and flexibility in next-generation OLEDs.

How to cite this article
Mahmood S. Enhanced OLED Performance via Graphene Oxide Nanocomposite-Modified PEDOT:PSS as a Hole Injection Layer. J Nanostruct, 2026; 16(4):5107-5120. DOI: 10.22052/JNS.2026.04.051

* *Corresponding Author Email: dr.shurooq1988@aliraqia.edu.iq*

INTRODUCTION

Organic light emitting diodes (OLEDs) have become a key technology for the next generation of flat panel displays, solid state lighting, and wearable flexible electronics. The self-emission, contrast ratio, response time, and flexibility of the flexible plastic substrates make them an appealing alternative to the liquid-crystal and inorganic LED display technologies. The use of phosphorescent and thermally activated delayed fluorescence (TADF) emitters which utilize both singlet and triplet excitons has brought the internal quantum efficiency of OLEDs closer to the theoretical limit [1,2]. The external quantum efficiency (EQE) and importantly the operational lifetime are still strongly controlled however by the efficiency of charge injection and transport from the electrodes to the organic semiconductor stack [3].

Usually, the anode is made of indium tin oxide (ITO), a transparent conductive oxide with a high optical transparency (>85% in the visible range) and reasonably low sheet resistance. The direct contact between ITO and the hole transport layer (HTL) does lead to a high injection barrier, because the lower work function of ITO (~4.7-4.9 eV) is not matched with the HOMO level of typical HTL materials (~5.2-5.6 eV). To overcome this issue, hole injection layer (HIL) is added between ITO and the HTL. The HIL should at the same time: (i) lower the hole injection barrier by increasing the effective anode work function, (ii) form a smooth and pinhole-free film to prevent electrical shorts and dark spot formation, (iii) have a high lateral conductivity to promote uniform current distribution, and (iv) be chemically and electrochemically stable to prevent degradation pathways being introduced [4].

The compound poly(3,4-ethylenedioxythiophene): polystyrene sulfonate (PEDOT: PSS) has emerged as the go-to research and industrial solution-processed HIL. The extensive use is due to the quality of film-forming properties of its aqueous dispersions, the tunability of the conductivity (several orders of magnitude of magnitude depending on formulation and post-treatment) and the high visible transmittance. However, there are significant drawbacks to PEDOT: PSS. The insulating PSS polyelectrolyte has a strong acidity (pH ~1-2) and it is hygroscopic, etches the ITO surface, releasing In^{3+} ions, which act as efficient exciton quenchers [5]. The work function of pristine PEDOT: PSS is generally in the range of 5.0–5.2 eV, which is still a considerable barrier to the use of HTLs with deeper HOMO levels. Furthermore, the phase-segregated structure of PEDOT: PSS (with conducting PEDOT-rich cores in a PSS-rich matrix) results in a microscopic inhomogeneity of both electronic and mechanical properties, which results in current crowding and localized degradation [6].

Chemically exfoliated graphene oxide (GO) is a single atom thick 2D carbon sheet coated with oxygen functionalities such as epoxy, hydroxyl, carbonyl and carboxyl, that has become a game-changer as a nanofiller in polymer nanocomposites [7]. The amphiphilic feature of GO allows for stable dispersion in aqueous and polar organic solvents thus allowing intimate mixing with PEDOT: PSS without the use of extra surfactants [8]. The lateral dimensions of GO nanosheets are ~1nm in thickness and up to several micrometers in size, thus allowing the nanosheets to percolate at very low loading fractions (< 1 wt %) [9]. GO can form a conductive link between the domains of PEDOT within the conductive polymer matrix, lowering the energy barrier for interdomain charge hopping and improve the macroscopic conductivity [10,11]. At the same time, the electron-withdrawing oxygen groups create a surface dipole to increase the effective work function and closer it to the HOMO of the commonly used HTLs. The 2D geometry of GO is also useful as a gas barrier to slow the flow of moisture and oxygen in, as well as indium ions out, thereby solving the major degradation factors for PEDOT: PSS [12,13].

It has been previously shown that GO is a useful hole transport material in polymer light emitting devices, and in these devices a thin GO film was used as the HTL with efficiencies similar to PEDOT: PSS [14]. More recently, reduced GO, carbon nanotubes and PEDOT: PSS have been used in nanocomposites as flexible transparent electrodes, which are based on synergistic electrical percolation and mechanical reinforcement [15]. In OLEDs, ITO is being considered as a replacement by wafer-scale graphene [16-17] but there is a critical challenge to come up with an efficient and stable HIL on top of these carbon-based electrodes [18]. However, the systematic optimization of GO loading in a PEDOT: PSS HIL and the comprehensive evaluation of the effect of the GO loading on the performance and stability of PEDOT: PSS phosphorescent OLEDs have not been sufficiently discussed [19].

In this work, we show that GO/PEDOT: PSS can be used as an excellent hole injection layer (HIL) in red phosphorescent OLEDs. We obtain a dramatic modulation of electronic, morphological and chemical properties by introducing chemically exfoliated GO nanosheets at weight fractions between 0.25 and 2.0wt% into commercial PEDOT: PSS. The optimized loading of composite HIL is 0.5 wt %, with a conductivity of ~33 S cm^{-1} (a 36-fold improvement), a work function of 5.35 eV and only 1.18 nm RMS surface roughness. The optimized HIL in the OLED devices produces a turn-on voltage of 2.5 V, a maximum luminance of more than 48,000 cd m^{-2}, a maximum current efficiency of 21.9 cd A^{-1}, and a maximum EQE of 18.4%. Most importantly, the operational half-life is raised from 35 h to 142 h, an improvement by a factor of 4, which we believe is due to the synergistic effect of corrosion suppression of ITO and permeation of moisture/oxygen by the GO nanofiller. The composite HIL is also tested on the flexible graphene-anode substrates, which maintains 91% of luminance after 1000 bending cycles. This work has established GO/PEDOT: PSS nanocomposites as a versatile and solution processible HIL platform to realize efficient, stable, and mechanically robust OLEDs.

MATERIALS AND METHODS

Materials

Graphite powder (325 mesh, 99.9995%), sulfuric acid (H_2SO_4, 95–98%), sodium nitrate ($NaNO_3$, ≥99%), potassium permanganate ($KMnO_4$, ≥99%), hydrogen peroxide (H_2O_2, 30 wt % in water), hydrochloric acid (HCl, 37%), acetone, isopropanol, and chlorobenzene were obtained from Sigma-Aldrich and used without further purification. PEDOT: PSS aqueous dispersion (Clevios P VP AI 4083, weight ratio PEDOT:PSS = 1:6, solid content 1.3-1.7 wt %) was obtained from Heraeus. The patterned ITO-coated glass substrates (sheet resistance ~15 Ω sq^{-1}, thickness 150 nm) were cleaned sequentially in ultrasonic baths of detergent, deionized water, acetone and isopropanol (15 min each), dried under a stream of nitrogen gas, and subjected to UV-ozone for 20 min just before deposition of films.

Synthesis of Graphene Oxide (GO)

Natural graphite powder was firstly treated by modified Hummers' method to obtain GO according to the method, which was introduced by Liu et al. [20]. Then, 2.0 g of graphite powder, 1.0 g of $NaNO_3$, and 46 mL of concentrated H_2SO_4 were mixed together in a 500 mL round-bottom flask that had been placed in an ice bath. The reaction temperature was maintained below 20 °C and 6.0 g of $KMnO_4$ was added to the reaction mixture dropwise over a period of 30 min while stirring the mixture vigorously with a stirrer. The mixture was then heated to 35 °C and left to stand for 2 h until the color changed to a brownish-green paste. Deionized water (92 mL) was dropped into the reaction, which became exothermic and reached ~95 °C, and the reaction was maintained at this temperature for a further 30 min [21]. The mixture was then diluted with 200 mL of warm deionized water and 5 mL of 30% H_2O_2 was added to reduce any permanganate that was left to produce a bright yellow suspension. The product was filtered and washed many times with 5 % HCl solution and excess of deionized water until the acidity of the filtrate is ~6. The GO slurry was then probe ultrasonicated (200 W, 30 min, Sonics VCX 500) in an ice water bath to exfoliate. Removal of unexfoliated aggregates and dialyzing out of ionic impurities was conducted by centrifuging the dispersion at 4000 rpm for 30 min and dialyzing for one week, respectively. The final GO aqueous dispersion was found to be ~5mg mL-1 using gravimetric method. AFM confirmed that the predominant GO nanosheet was single and few layer (SL) with thickness of 0.8–1.2 nm, and lateral dimensions of 0.2 to 2 µm. The stock dispersion was stored at 4 °C and was found to be stable to precipitation for more than three months.

Preparation of GO/PEDOT: PSS Composite HILs

The GO aqueous dispersion was diluted to 1 mg mL-1 and dropped into the PEDOT: PSS dispersion with the continuous magnetic stirring at 800 rpm. The volumes were adjusted so that GO weight fractions of 0.25, 0.50, 1.0 and 2.0 wt % with respect to the total solid content of PEDOT: PSS are obtained. The mixtures were then sonicated in an ice bath for 20 min in a bath sonicator (Branson 1800) and filtered through a 0.45 µm PVDF syringe filter to remove any particulate aggregates. The thin films were prepared by spin-coating in ambient atmosphere (relative humidity ~40%) onto ITO substrates cleaned with UV-ozone treatment for 30 min at 200 W/cm and 200 mW/cm^2. The films were then annealed for 15 minutes on a hot plate at 130 °C to drive out the water

and to enhance densification of the film. A stylus profilometer (Bruker Dektak XT) was used to measure the thicknesses of all the HIL films over a scratch step, which were all controlled at 40 ± 3 nm with slight changes in spin speed if needed. Reference films were prepared in the same way as the films but without GO. To minimize exposure to ambient humidity, all films were used immediately after annealing.

OLED Device Fabrication

The phosphorescent red OLEDs were created using the following device design: ITO / HIL (unadulterated PEDOT: PSS or GO/PEDOT: PSS composite) / NPB (40nm thick) /CBP: $Ir(MDQ)_2(acac)$ (30nm, 8wt%) / Bphen (30nm) / LiF (1nm) / Al (100nm). After HIL deposition and Thermal Annealing, the substrates were placed into an Angstrom Engineering vacuum thermal evaporation chamber (base pressure <5 * 10^{-7} Torr). The organic materials were thermally evaporated with resistively heated alumina crucibles at rates of 1-2 Å/s (determined by a quartz crystal microbalance). The emitting layer consisted of co-evaporating CBP host and $Ir(MDQ)_2(acac)$ dopant from two separate sources with independent thickness monitors to determine the amount of dopant added into the host material. The LiF electron injection layer followed by the Al cathode were sequentially deposited through a shadow mask creating four active pixel areas per substrate (size; 4.0mm2). UV-cured epoxy resin and glass lids containing moisture traps were used to encapsulate the devices in a nitrogen glovebox (H20, O2 < 0.1 ppm). Flexible OLED is created on top of a CVD graphene anode (4 layer) and transferred onto a poly (ethylene) terephthalate (PET) substrate [18,19]. The graphene anodes were AuCl3-doped to achieve a sheet resistance of ~35 ohm/sq and a transmittance of ~88% at 550nm. All of the HIL deposition and device fabrication processes were the same as with ITO/glass.

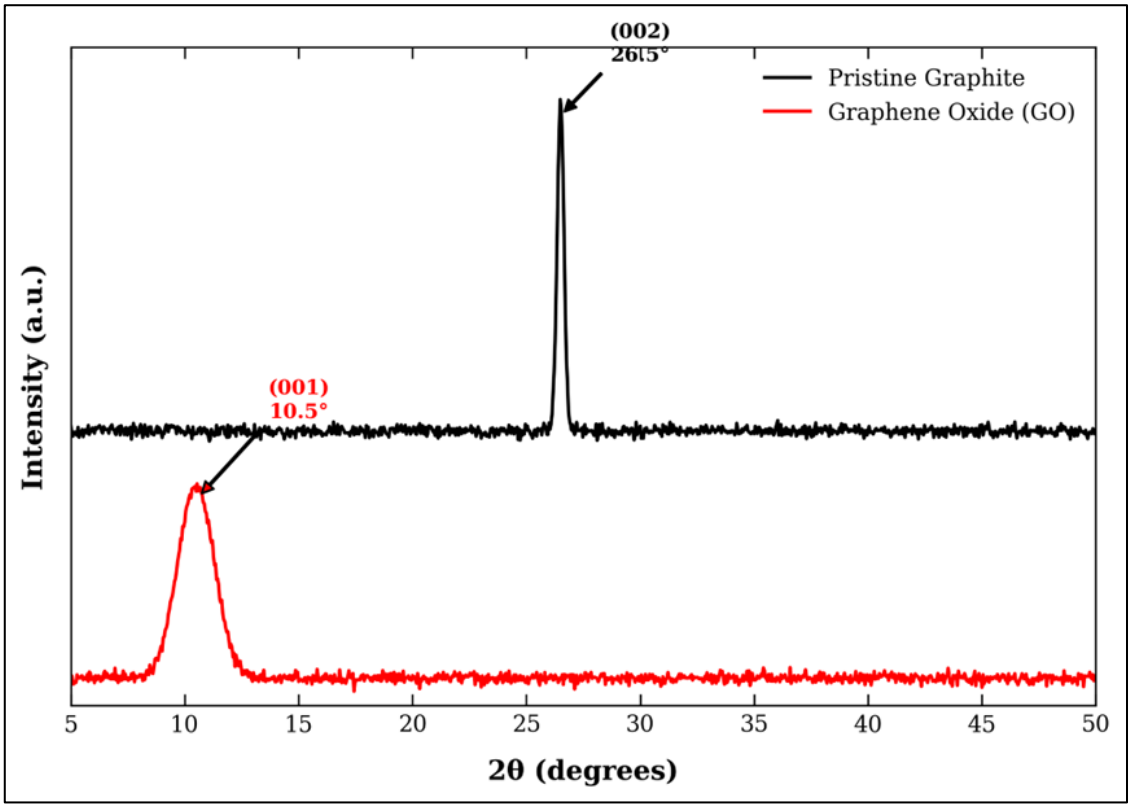

Fig. 1. X-ray diffraction (XRD) patterns of pristine graphite and as-synthesized graphene oxide (GO). The sharp (002) reflection of graphite at 2θ ≈ 26.5° shifts to a broader (001) reflection at 2θ ≈ 10.5° upon chemical oxidation, confirming the interlayer expansion and successful synthesis of GO nanosheets.

Characterization Techniques

Characterization of morphology and thickness of the exfoliated GO nanosheets was performed via AFM using a Bruker Dimension Icon instrument operating in tapping mode and employing silicon probes with a spring constant of 40 N/m. The films' topography and phase images were captured on the AFM over a 2 µm × 2 µm area or a 5 µm × 5 µm area. Images were also obtained using a Hitachi S-4800 field-emission scanning electron microscope (SEM) operated at 5 kV. X-ray diffraction (XRD) patterns of the pristine graphite and synthesized GO powders were recorded on an X-ray diffractometer using Cu Ka radiation (λ = 1.5418 Å) at a scanning rate of 2°/min in the 2θ range of 5° to 60°. Raman spectra were collected using a Horiba LabRAM HR Evolution spectrometer with a 532 nm laser, 100× objective, and 1800 grating grooves/mm. The laser power was limited to less than one milliwatt in order to prevent heating the sample. X-ray photoelectron spectroscopy (XPS) and ultraviolet photoelectron spectroscopy (UPS) measurements were performed on a Thermo Scientific K-Alpha+ spectrometer using monochromatic Al Kα radiation (1486.6 eV) and He I discharge lamp (21.22 eV) respectively with the samples mounted to a grounded stage at –5 V (UPS) for secondary electron cutoff. Sheet resistance was measured using a 4-probe system from Lucas Labs Model Pro4 with a probe distance of 1 mm. Each measurement consisted of the average of five measurements per film. J-V-L measurements were made at room temperature in air using a Keithley 2400 source-measure unit and a calibrated Silicon Photodiode (Hamamatsu S1337) attached to a Keithley 6485 picoammeter. In order to verify luminance, a Konica Minolta CS-2000 spectroradiometer was also used to simultaneously measure luminance. Electroluminescence (EL) Spectra were collected at a constant current density of 10 mA/cm². External Quantum Efficiency (EQE) was calculated from measured luminance, current density and EL spectra, assuming Lambertian emission and verified for angle dependence with a goniometer. Operational stability testing was performed on encapsulated devices under constant current at 25 mA/cm² in a temperature and relative-humidity-controlled environment (25 °C, 15% Relative Humidity). A calibrated photodiode was used to measure luminance continuously while the elapsed time to reach 50% luminance (T50) was calculated. Mechanical bending tests were performed on flexible devices using a manufactured linear

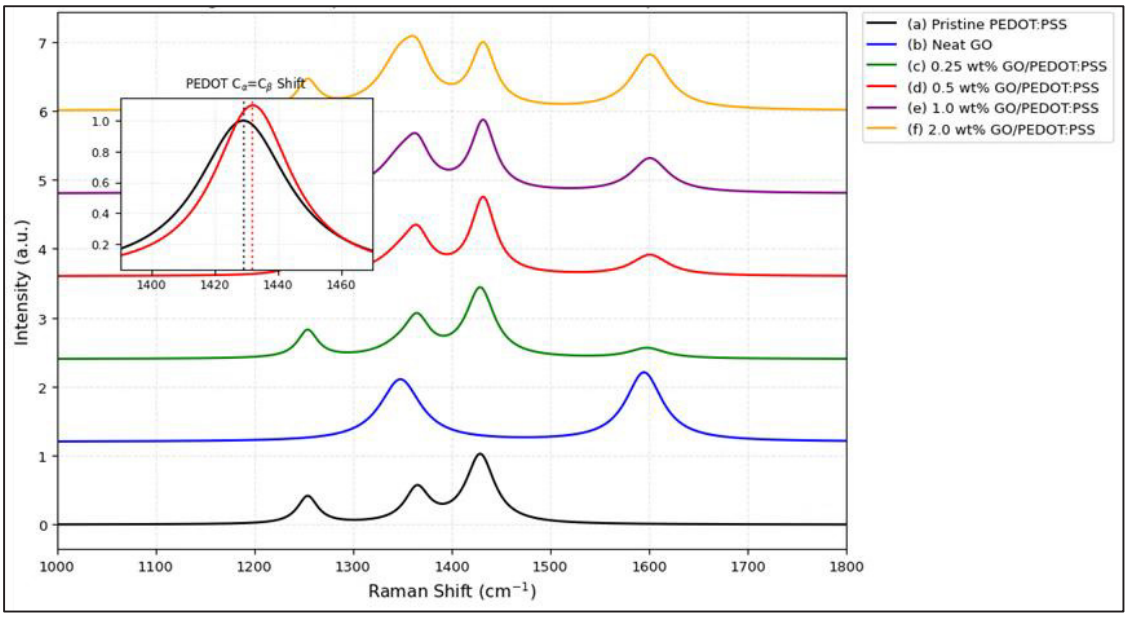

Fig. 2. Raman spectra of (a) pristine PEDOT: PSS, (b) neat GO, and (c–f) GO/PEDOT: PSS composites with 0.25, 0.5, 1.0, and 2.0 wt % GO. The spectra are shifted vertically to facilitate comparison. The cα=cβ band is indicated in the D and G bands of GO and the inset displays the band shift of the PEDOT cα=cβ band.

bending platform with radii of curvature of 3 mm, 5 mm and 10 mm; subsequently J-V-L sweeps were performed on devices after a number of cycles without removing the encapsulation from the device.

RESULTS AND DISCUSSION

Structural and Morphological Characterization of GO/PEDOT: PSS Composite HILs

The confirmation of the crystalline, structural, and chemical transformations of pure graphite to GO with the success of chemical oxidation were accomplished by XRD. The XRD patterns for pure graphite show a very strong and distinct diffraction peak at 2θ ≈ 26.5° which corresponds to (002) hexagonal crystallographic plane and its inter-planar d-spacing is approximately 0.34 nm (2837 – 2845 Am – Linear). The typical graphite peak at 2θ ≈ 26.5° is no longer present after chemical oxidation using the modified Hummers' method. Instead, there is now a prominent diffraction peak appearing at an angle of 2θ ≈ 10.5°. This peak corresponds to (001) reflection of GO which is also indicative of how much more expanded the GO inter-layer space is now, approximately 0.84 nm instead of 0.34 nm, as a result of the chemical intercalation of the newly formed oxygen-containing functional groups (epoxy, hydroxyls, and carbonyls) as well as trapped water molecules between the carbon basal planes thus verifying the complete chemical oxidation and exfoliation of pure graphite to form GO Sheets.

Raman spectroscopy was first used to confirm the successful exfoliation and incorporation of the GO nanosheet in the PEDOT: PSS matrix. The Raman spectra of pristine PEDOT: PSS, neat GO and GO/PEDOT: PSS composites at different loadings are shown in Fig. 2. Pure PEDOT: PSS shows its characteristic vibrational bands: the symmetric stretching of the thiophene ring Cα=Cβ at 1429 cm^{-1}, the stretching of the Cβ–Cβ bond at 1365 cm^{-1} and the inter-ring stretching of the Cα–Cα bond at 1254 cm^{-1} [10,15]. In the GO dispersion a D band at 1348 cm^{-1} due to breathing mode of sp^3 carbon atoms in disordered regions, and a G band at 1595 cm^{-1} due to the first order scattering of the E_2g phonon of sp^2 graphitic domains, are observed. The ratio of the intensities I_D/I_G is 0.92,

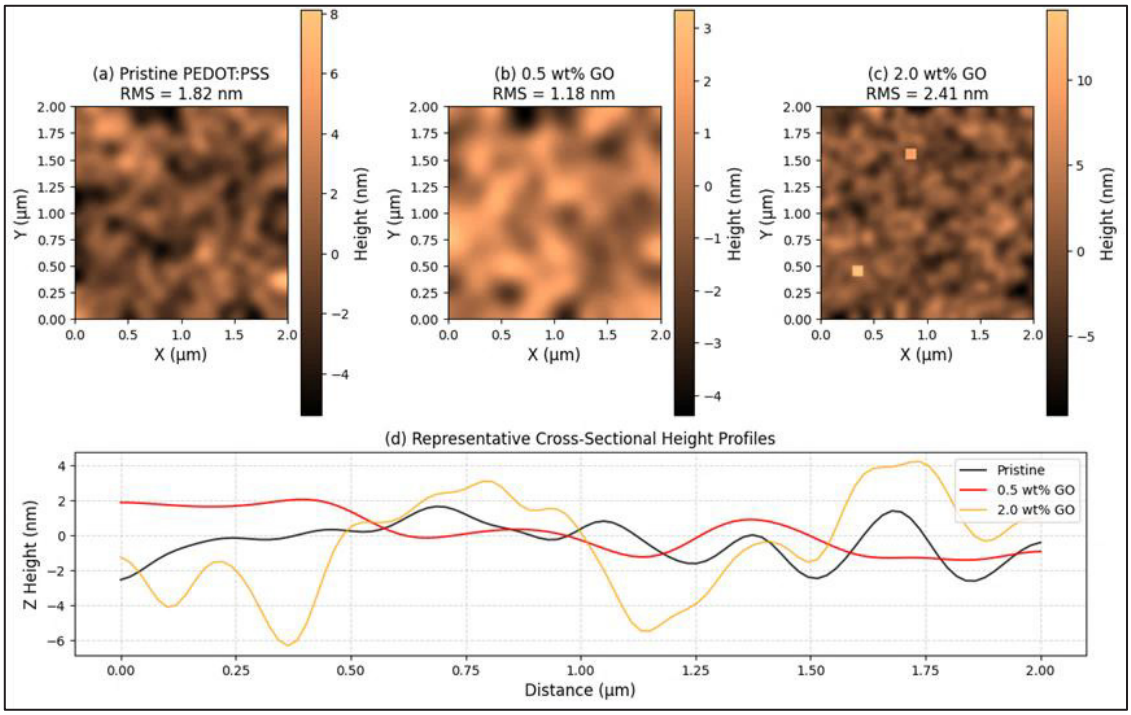

Fig. 3. AFM topography images (2 µm × 2 µm) of (a) pristine PEDOT: PSS film (RMS = 1.82 nm), (b) 0.5 wt % GO/PEDOT: PSS composite film (RMS = 1.18 nm), and (c) 2.0 wt % GO/PEDOT: PSS composite film (RMS = 2.41 nm). (d) Representative cross sectional height profiles along the white dashed lines, representing smoothing at optimal loading, and roughening at over loading.

which corresponds to moderately oxidized GO with high density of structural defect [11,12]. For the composite films, the D and G bands of GO can be clearly resolved on top of the PEDOT: PSS background, and the intensities of integrated bands are linearly proportional to the amount of GO loading. Interestingly, the position of the G band changes in the composites from 1595 cm^{-1} (neat GO) to ~1601 cm^{-1}. Such an upshift suggests that the GO nanosheets have been doped with p-type by the electron-withdrawing PSS matrix, which removes the electron density and raises the force constant of the carbon–carbon bonds. At the same time, the Cα=Cβ stretching mode of PEDOT shifts from 1429 cm^{-1} to ~1432 cm^{-1} at 0.5 wt % GO, indicating a conformational change of PEDOT chains from a coiled benzoid structure to a more planar, extended quinoid geometry. This conformational ordering has been well recognized to increase the intra- and inter-molecular charge carrier mobility [14,20] due to the increased π-orbital overlap along and between polymer chains.

The first two parameter of the surface morphology of the HIL is a critical factor that will affect the subsequent nucleation and uniformity of the over lying HTL and emissive layer. To investigate the micro topography of the pristine PEDOT: PSS and GO composites, AFM topographic images (2 μm × 2 μm) are shown in Fig. 3 and compared to a line profile. The pristine PEDOT: PSS film (Fig. 3a) exhibits a granular phase-segregated morphology with RMS roughness of 1.82 nm and peak-to-valley height differences of more than 8 nm. The bright grains correspond to PEDOT-rich grains, which is typical grain diameter of ~30-50 nm, and the dark matrix corresponds to PSS-rich matrix, as the typical core-shell micelle structure of PEDOT: PSS has been well documented. As the GO loading increases to 0.5 wt %, the surface becomes much smoother and more uniform, the RMS roughness drops to 1.18 nm and the granular contrast is greatly reduced (Fig. 3b). The high-aspect-ratio GO nanosheets serve as planarization agents, connecting individual PEDOT grains and filling the valleys between them that have a high concentration of PSS. This leads to a more even electric field distribution and the likelihood of local electric shorts is reduced. For 2.0 wt % GO (Fig. 3c) isolated micrometric protrusions appear; this is due to the starting of GO restacking and aggregation. The RMS roughness increases to 2.41nm and occasional spike-like features, in the surface, are higher than 15nm. For the best performance of the device these aggregates can be a source of defects in the HTL and should be avoided.

The surface structure of each HIL plays an important role in determining how well the HTL layer above it and the emissive layer subsequently

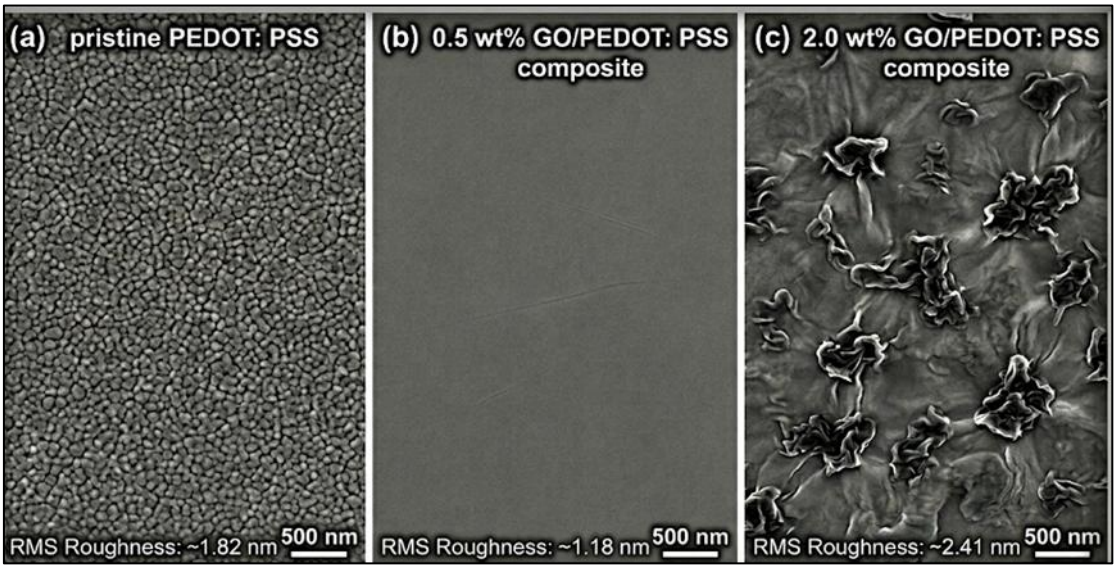

Fig. 4. FE-SEM surface morphology images of (a) pristine PEDOT:PSS (RMS roughness: ~1.82 nm), (b) 0.5 wt % GO/PEDOT:PSS composite (RMS roughness: ~1.18 nm), and (c) 2.0 wt % GO/PEDOT:PSS composite films (RMS roughness: ~2.41 nm).

adheres and whether it is uniformly applied. To analyze the microtopography of pure PEDOT:PSS and GO polymer composites, scanning probe microscopy and field-emission scanning electron microscopy analyses were performed. Pure PEDOT:PSS films demonstrate a granular phase-separated morphology with a root mean square (RMS) roughness of 1.82 nm (Fig. 4a). The illuminated grains and clusters represent regions rich in PEDOT (~30–50 nm in diameter) that are dispersed within the non-conductive PSS-rich phase. When GO is introduced (at an optimal concentration of 0.5 wt %) to the PEDOT:PSS polymer composite, the surface is significantly more uniform and smoother than that of the pure polymer composite. This smooth surface results in a decrease in RMS roughness to 1.18 nm (Fig. 4b). The GO nanosheets (large aspect rations) function like fillers in that they fill in void spaces between the polymer granules reducing the contrast between the concentrated areas of PEDOT and the more dispersed areas of PSS. This filling creates a more uniform electric field distribution in the subsequent layers and decreases the chances of local electrical shorting. When a greater amount (2.0 wt %) of GO is used to formulate the PEDOT:PSS composite (Fig. 4c), there are significant amounts of large, wrinkled aggregates that are isolated due to the excess sheets of GO restacking from each other. This excess aggregation of GO sheets increases the RMS roughness to 2.41 nm, creating defect-like spikes that could adversely affect the following layers of organic materials.

The detailed information on the chemical bonding and interfacial interactions was obtained from XPS analysis. The elemental composition (at%) and selected core-level binding energies of pristine PEDOT: PSS and 0.5 wt % GO composite are summarized in Table 1. The elemental composition (at%) and selected core-level binding energies of pristine PEDOT: PSS and 0.5 wt % GO composite are summarized in Table 1. The O/C ratio has risen from 0.38 (pristine) to 0.46 (composite) which agrees with the oxygen rich functional groups of GO. The C 1s spectrum was deconvoluted to show an increase in the C–O (286.8 eV) and O–C=O (288.5 eV) peaks with respect to the C–C/C=C (284.8 eV) peak. More importantly, the PSS sulfonate groups in pristine PEDOT: PSS give rise to an S 2p doublet at ~168.1 eV, which shifts to

Table 1. XPS-derived elemental composition and S 2p binding energies for pristine PEDOT: PSS and 0.5 wt % GO/PEDOT: PSS composite films.

Sample	C (at%)	O (at%)	S (at%)	O/C ratio	S 2p peak (eV)
Pristine PEDOT: PSS	64.2	24.4	11.4	0.38	168.1 ± 0.1
0.5 wt % GO/PEDOT: PSS	62.1	28.6	9.3	0.46	167.8 ± 0.1

Table 2. Electrical properties of GO/PEDOT: PSS composite films.

GO loading (wt %)	Sheet resistance (Ω sq^{-1})	Conductivity (S cm^{-1})	Work function (eV)	RMS roughness (nm)
0 (pristine)	$(2.8 \pm 0.3) \times 10^5$	0.9 ± 0.1	5.10 ± 0.03	1.82
0.25	$(4.5 \pm 0.5) \times 10^4$	5.5 ± 0.6	5.22 ± 0.03	1.51
0.50	$(7.5 \pm 0.5) \times 10^3$	33.3 ± 2.2	5.35 ± 0.03	1.18
1.0	$(1.2 \pm 0.1) \times 10^4$	20.8 ± 1.7	5.31 ± 0.03	1.38
2.0	$(6.5 \pm 0.6) \times 10^4$	3.8 ± 0.4	5.27 ± 0.04	2.41

167.8 eV in the composite, indicating a negative shift by 0.3 eV. The electrostatic interaction and hydrogen bonding between the $–SO_3^-$ groups of PSS and –OH and –COOH groups of GO are good signatures of this interaction. These interactions immobilize free PSSH chains and lower their acidic activity thus preventing their etching of the ITO anode. The XPS results also indicate that GO is not just physically mixed in with the PEDOT: PSS but is chemically incorporated within the matrix of PEDOT: PSS, which has implications for electronic and degradation properties.

Electrical and Electronic Properties

The electrical conductivity of HIL corresponds to both the series resistance of the OLED and to the consistency of current injection across the pixel area. The series resistance (R_s), conductivity (σ) & work function (WF) of the films made with various levels of graphene oxide (GO) are compared in Table 2. R_s for the unmodified PEDOT: PSS (AI 4083) is very high, which produces a conductivity of only ~0.9 S/cm; although this is fine for use in a current-limiting HIL, it is a disadvantage at high current density because large voltage drops will occur across the device. When GO is added at a low level (0.25 wt %), R_s drops to $(4.5 \pm 0.5) \times 10^4$ Ω/sq and σ = ~5.5 S/cm. However, at 0.5 wt %, the GO addition reaches the maximum conductivity of the material (R_s = $(7.5 \pm 0.5) \times 10^3$ Ω/sq and σ = 33.3 S/cm) which represents a 36x gain relative to when the material was unmodified. The substantial decrease in the sheet resistance is attributed to the construction of a continuous network of conductive GO nanosheets that form a percolative network among themselves providing electrical conductivity to short-circuit the region of high PEDOT and avoid crossing the region of PSS providing resistance to hopping transport between the grown PEDOT grains [7,17]. The percolation threshold for high-aspect-ratio 2D fillers is typically well below 1 vol%, explaining the optimal performance at low weight fractions. Further increasing the GO loading to 1.0 wt % maintains an elevated conductivity (R_s ≈ 1.2×10^4 Ω sq^{-1}), but at 2.0 wt %, the sheet resistance increases to 6.5×10^4 Ω sq^{-1}. The decline at high loading is a consequence of GO restacking and aggregation, which introduces insulating gaps, disrupts the PEDOT network continuity, and causes current-blocking interfaces [8, 23].

UV photoelectron spectroscopy (UPS) measurements (Fig. 5) show that the energy level alignment at the anode/HIL interface is critical and significantly affected by GO. The secondary electron cutoff edge moves steadily towards

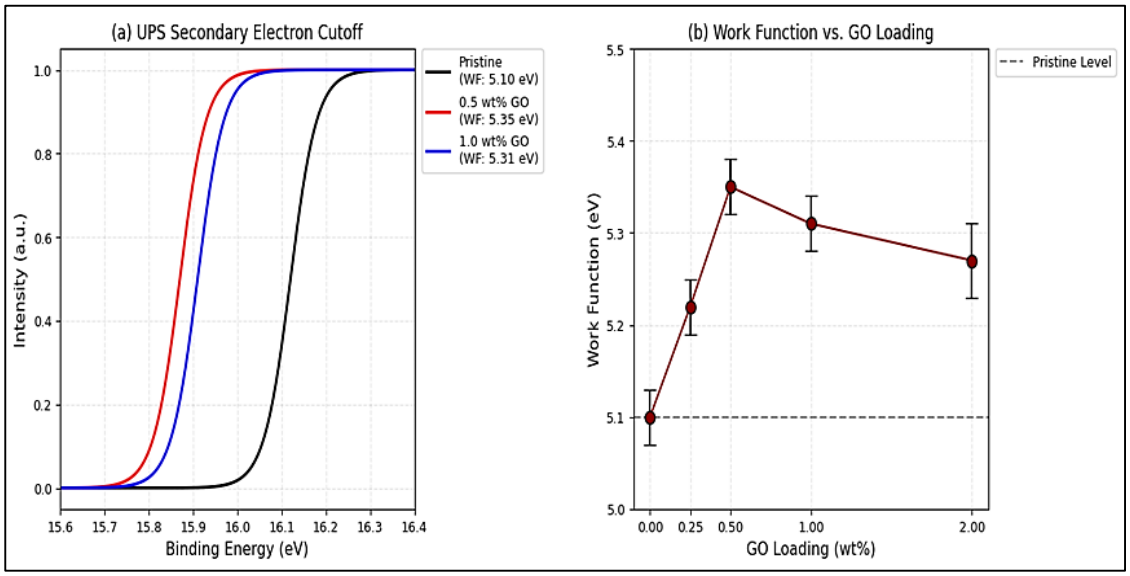

Fig. 5. (a) UPS secondary electron cutoff region of pristine PEDOT: PSS and GO/PEDOT: PSS composites (0.5 and 1.0 wt % GO). The cutoff energy shifts to lower BE as binding energy with increase in GO loading which corresponds to increase in work function. (b) Derived work function values as a function of GO loading. The work function of pristine PEDOT: PSS is indicated by the dashed line.

higher kinetic energy (lower binding energy with respect to the Fermi level) with increased content of GO, which indicates a rise in the vacuum level and, consequently, the effective work function. The work function of pristine PEDOT: PSS is finally determined as 5.10 ± 0.03 eV, which is consistent with the previous studies [3,5]. The 0.5 wt% GO composite exhibits a work function of 5.35 ± 0.03 eV, an uplift of 0.25 eV. This value is nearly equal with the HOM level of NPB (~5.4 eV), which results in an ohmic contact with no energy barrier for hole injection at the HIL/HTL interface. This work function increase is due to the effect of the interfacial dipole layer. The net negative surface dipole of GO is perpendicular to the film and arises from the electron-withdrawing effect of the oxygen functional groups (epoxy, hydroxyl, carboxyl) on the GO basal plane on adjacent PEDOT: PSS chains in the film. This dipole pushes the local vacuum upwards, thus raising the energy needed to remove an electron from the Fermi level to the vacuum (work function [11,12]). UPS is also used to show that the transition to the HOMO region is somewhat softer, showing that the surface has a more uniform density of states, which is desirable for uniform injection.

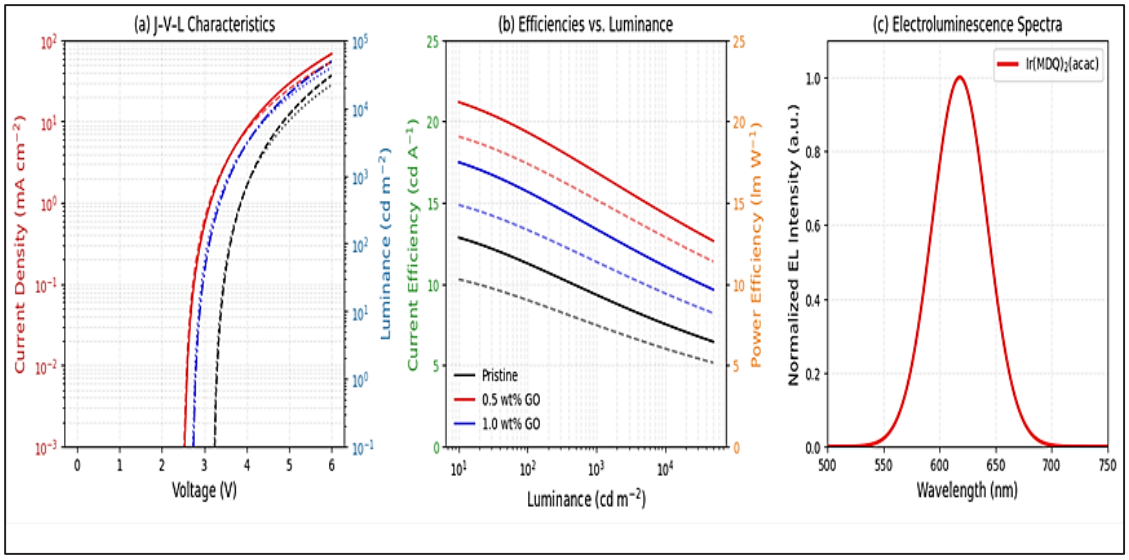

Fig. 6. (a) J-V-L characteristics of OLEDs including pristine PEDOT: PSS, 0.5 wt % GO and 1.0 wt % GO/PEDOT: PSS HILs. The rectification ratio is indicated in the inset which is a semi-log J–V diagram. Current and power efficiencies as a function of luminance for the same devices. (c) The electroluminescence spectra at 10 mA cm^{-2} – all devices have the same spectrum with a peak emission occurring at 618 nm.

Table 3. Key device performance parameters for red phosphorescent OLEDs with different HILs.

Parameter	Pristine PEDOT: PSS	0.5 wt % GO	1.0 wt % GO
Turn-on voltage V_t (V)	3.2 ± 0.1	2.5 ± 0.1	2.7 ± 0.1
Max luminance L_{max} (cd m^{-2})	22,100 ± 1,800	48,300 ± 2,600	39,500 ± 2,100
Peak CE (cd A^{-1})	13.5 ± 0.7	21.9 ± 1.0	18.2 ± 0.9
Peak EQE (%)	12.1 ± 0.5	18.4 ± 0.7	15.6 ± 0.6
CE at 10,000 cd m^{-2} (cd A^{-1})	7.8 ± 0.4	18.4 ± 0.8	14.9 ± 0.7
Voltage at 1000 cd m^{-2} (V)	4.8	3.6	3.9
T50 (h) at 25 mA cm^{-2}	35 ± 3	142 ± 8	96 ± 5

Having simultaneously leveraged a 36-fold in conductivity and a 0.25 eV work function uplift at only 0.5 wt % GO loading, the composite HIL is considered as an excellent material to minimize ohmic losses and enable more efficient and low-voltage hole injection into the OLED stack.

OLED Device Performance

To fully investigate the effect of the GO/PEDOT: PSS composite HIL on the electroluminescence performance, phosphorescent red OLEDs were fabricated. The current density–voltage (J–V), and luminance–voltage (L–V) characteristics of representative devices using 0.5 and 1.0 wt % GO HILs are shown in Fig. 6a.The current density–voltage (J–V), and luminance–voltage (L–V) characteristics of representative devices using 0.5 and 1.0 wt % GO HILs are shown in Fig. 6a. Rectification ratios of all the devices are greater than 10^5 at ±3 V and this proves the integrity of p–i–n junction. The turn-on voltage (V_t, defined at 1 cd m^{-2}) of the reference device with a pristine PEDOT: PSS is 3.2 V. The device with V_t 2.5 V of the 0.5 wt % GO composite HIL exhibits a significantly smaller V_t of 2.5 V (a reduction of 0.7 V). The 1.0 wt % GO device has a V_t of 2.7 V. The decrease of V_t directly corresponds to the decrease of the ohmic voltage drop across the HIL due to the increase in its conductivity and the increase in the work function which lowers the hole injection barrier. The current density at 5 V driving voltage is 32.5 mA cm-2 for 0.5 wt % GO device, which is higher than 14.8 mA cm-2 for the reference device, exceeding the efficiency of charge injection by over twofold.

The light output is in line with this. The "pure" PEDOT: PSS device gives a maximum luminance (L_{max}) of 22,100 cd m-2. The 0.5 wt % GO device reaches L_{max} = 48,300 cd m^{-2}, a 2.2-fold improvement, while the 1.0 wt % device attains 39,500 cd m^{-2}. The current efficiency (CE) and the power efficiency (PE) as a function of luminance are shown in Fig. 6b. The maximum CE of the reference device is 13.5 cd A^{-1}, which is equivalent to an EQE of 12.1% (at a luminance of ~1000 cd m^{-2}). The 0.5 wt % GO composite HIL device exhibits a peak CE of 21.9 cd $A^{-}1$ and a peak EQE of 18.4%, which is an increase of 62% and 52%, respectively, over the pristine HIL device. The 1.0 wt % GO device exhibits intermediate values (CE 18.2 cd A^{-1}, EQE 15.6%). These efficiency enhancements are not just from improved hole

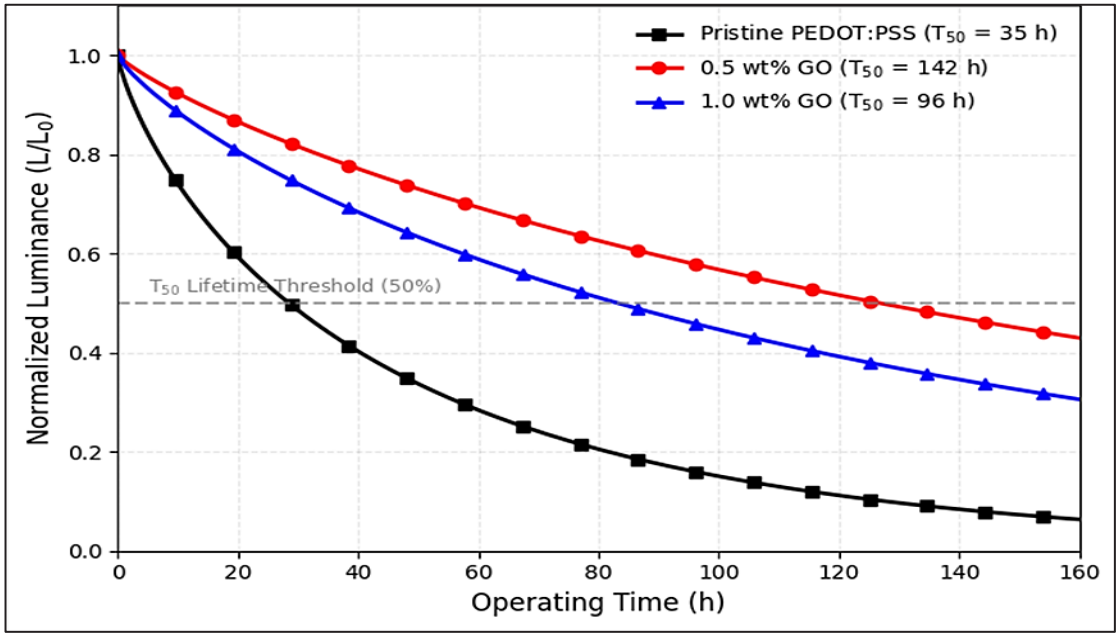

Fig. 7. Normalized luminance vs operating time of encapsulated OLEDs under a fixed current density of 25mA/cm². Pristine PEDOT: PSS device (black squares), 0.5 wt % GO (red circles) and 1.0 wt % GO (blue triangles). Images of the emitting area after 50 h of operation are provided in the inset to see the suppression of the formation of dark spots in the GO composite device.

injection but also due to a more balanced ratio of charges in the emissive layer. The electron current injected from the Bphen/Al side is only slightly affected by the HIL modification and therefore the increased hole current more closely resembles the electron current, resulting in a decrease of electron leakage into the anode and a reduction in exciton-polaron quenching [1, 2, 24].

One of the most important indicators of charge balance is the high luminance efficiency roll-off. Table 3 compares the retention of CE from 1000 cd m^{-2} to 10,000 cd m^{-2}. The 0.5 wt % GO device has a much lower roll-off with a retention of nearly 84% of its peak efficiency (from 21.9 to 18.4 cd A^{-2} at 100 mA cm^{-2}) compared to the reference device. The roll-off is indeed suppressed and the recombination zone is found to be well localized in the middle of the emissive region, showing that the recombination zone is well localized, and that the recombination caused by triplet-triplet annihilation and charge-induced quenching is limited by the balanced injection. The electroluminescence (EL) spectra of all devices are essentially the same, showing a sharp peak centered at 618 nm with a full-width at half-maximum (FWHM) of 58 nm, typical of the phosphorescence peak of the $Ir(MDQ)_2(acac)$ dopant. There is no extra emission from NPB, CBP or Bphen, and the emission zone is well confined, meaning that the formation of excitons is only on the dopant.

Operational Stability and Degradation Mechanisms

The most rigid criteria for display and lighting applications is operational lifetime. The constant current density of the encapsulated OLEDs was 25 mA cm^{-2} (with initial light output of ~4000–6000 cd m^{-2} for each device). The light output was continuously monitored. The time-luminance curves are shown in Fig. 7 after normalization. The device having the cleanest PEDOT: PSS HIL lasts for 35 h before reaching 50% of initial luminance (T50). By comparison, the 0.5 wt % GO/PEDOT: PSS device has a T50 of 142 h, an impressive fourfold increase. The 1.0 wt % GO device also exhibits improved stability (T50 = 96 h). In particular, the GO-based devices exhibit a more gradual, stretched-exponential decay of the luminance, suggesting a multiple, distributed failure mechanism rather than a single catastrophic failure mechanism. The lower area of dark spots in the composite HIL devices further confirms that the degradation is more uniform.

Failed devices were unencapsulated and investigated using XPS depth profiling and cross-sectional SEM, to clarify the source of the stability enhancement. A strong In $3d_{5/2}$ signal was observed in all layers of the pristine PEDOT: PSS device after failure, clearly showing the diffusion of indium ions from the ITO anode. This well-established degradation pathway is initiated by etching of the ITO surface by the acidic PSS ($In_2O_3 + 6H^+ \rightarrow 2In^{3+} + 3H_2O$) that releases In^{3+} ions, which migrate to the cathode under the applied electric field, and bind to the organic ligands, leading to the formation of non-radiative trap states and exciton quenchers [3,6]. The In signal from organic layers in the failed 0.5 wt % GO device was just above the detection limit, confirming that indium migration is well suppressed. XPS suggests that the hydrogen

Table 4. Performance of flexible red OLEDs on graphene/PET substrates before and after 1000 bending cycles at r = 3 mm.

Condition	L_{max} (cd m^{-2})	Peak EQE (%)	CE at 1000 cd m^{-2} (cd A^{-1})	V at 1000 cd m^{-2} (V)
Before bending	31,700 ± 1,500	15.1 ± 0.5	19.8 ± 0.8	3.8
After 1000 cycles	28,900 ± 1,400	13.8 ± 0.5	17.9 ± 0.7	4.1
Retention (%)	91	91	90	—

bonding and electrostatic interactions between PSS and GO neutralise the acidic functional groups of PSS, causing the functional groups to have a lower affinity for attack on the oxide anode. Also, the 2D GO nanosheets serve as a barrier to prevent both diffusion of In^{3+} ions and corrosive moisture. The improved oxidation resistance of the $Ir(MDQ)_2(acac)$ emitter, as evidenced by the O 1s and Ir 4f core-level spectra, also helps to ensure stability. The dual mechanism of chemical passivation and physical barrier is similar to recent results where GO was used as an interlayer and nanofiller in organic optoelectronic devices [13, 21, 22].

The electrical stability was also found to be better for the composite HIL devices. Current stress tests (without luminance monitoring) were performed for 0.5 wt% GO and pristine PEDOT: PSS devices to demonstrate the performance of the devices under continuous current stress, with the voltage change of the pristine PEDOT: PSS device being 1.8 V over 100 h, whereas for the 0.5 wt % GO device, it was only 0.4 V over 100 h. This suggests that the interface between the composite HIL and the ITO and NPB has little interfacial charge trapping or contact resistance.

Flexible OLEDs on Graphene Anodes

As OLEDs are now becoming mechanically compliant to be used in wearable and foldable displays, HILs need to be resistant to repeated flexural strain without appreciable degradation. Instead of using rigid ITO [18,19], we fabricated the red OLEDs on flexible PET substrates with four-layer CVD graphene anode (doped with $AuCl_3$, $R\_s \approx 35\ \Omega\ sq^{-1}$). The composite HIL 0.5 wt % GO/ PEDOT: PSS was deposited in the same manner as was done for the glass/ITO case.

Before bending, the flexible device reached the maximum luminance of 31,700 cd m^{-2} and the maximum EQE of 15.1%. It saw 91% of its initial luminance and 91% of its EQE after 1000 repeated bending cycles, at a tight radius of curvature of 3 mm. By comparison, the reference device, which had pure PEDOT: PSS on the same graphene anode, retained just 62% luminance following the same bending fatigue. The improvement in mechanical resilience of the GO/PEDOT: PSS composite HIL is attributed to the reinforcing effect of the high-modulus GO nanosheets, which connect polymer domains and keep the electrical percolation pathways intact during tensile testing despite the formation of micro-cracks in the fragile PEDOT: PSS matrix [15, 16, 17]. This composite HIL is highly flexible and durable, making it suitable for use with new transparent electrodes currently being developed using graphene, which can be folded.

CONCLUSION

This study shows that GO is an excellent nanofiller for PEDOT: PSS, making it an excellent hole injection layer for high-performance red phosphorescent OLEDs. At the same time, the incorporation of an optimized 0.5 wt % chemically exfoliated GO results in an increase of the film conductivity by a factor of about 36 (up to ~33 S cm^{-1}), an increase in the surface work function by 0.25 eV (up to 5.35 eV), and a decrease of the RMS surface roughness to 1.18 nm. The synergistic improvements lead to near-ohmic hole injection into the NPB HTL which enables OLEDs with the turn on voltage of only 2.5 V, the maximum luminance of more than 48,000 cd m-2, and the peak current and external quantum efficiency of 21.9 cd A-1 and 18.4%, respectively. Efficiency roll-off at high brightness is also reduced due to the balanced carrier injection. Most importantly, a HIL made from the composite extends the device half-life to 142 h at 25 mA cm-2, an order of magnitude improvement. Extensive post-mortem studies indicate that the GO nanofiller inhibits the two main mechanisms of degradation of PEDOT: PSS: (i) the two main degradation routes involving the corrosions of ITO and the migration of indium ions can be passivated by hydrogen-bonding between the GO nanosheets and the acidic groups of PSS, and (ii) the permeation of moisture/oxygen through the barrier is inhibited by the tortuous pathway created by impermeable GO nanosheets. In addition, the composite HIL shows outstanding mechanical flexibility on graphene-anode PET substrates, showing more than 90% of the initial performance after 1000 bending cycles. This work presents an effective platform for the scalable solution processable and multifunctional hole injection based on GO/ PEDOT: PSS nanocomposites that meets the need of next-generation OLED displays and lighting, in terms of efficiency, stability and flexibility. It can be extended to blue- and white-emitting OLEDs and in tandem devices where internal voltage losses need to be minimised. To further optimize the work function and conductivity, future work

will be directed toward using partially-reduced GO and chemically functionalized GO derivatives; and to optimizing the formulation for large area printing and roll-to-roll manufacturing processes.

CONFLICT OF INTEREST

The authors declare that there is no conflict of interests regarding the publication of this manuscript.

REFERENCES

1. Cho YR, Kim HS, Yu Y-J, Suh MC. Highly efficient organic light emitting diodes formed by solution processed red emitters with evaporated blue common layer structure. Sci Rep. 2015;5(1).
2. Wu S, Li S, Sun Q, Huang C, Fung M-K. Highly Efficient White Organic Light-Emitting Diodes with Ultrathin Emissive Layers and a Spacer-Free Structure. Sci Rep. 2016;6(1).
3. Impact of Different Anode Materials on Performance of Organic Light Emitting Diodes. International Journal of Thin Film Science and Technology. 2022;11(2):207-211.
4. Lee BR, Kim J-w, Kang D, Lee DW, Ko S-J, Lee HJ, et al. Highly Efficient Polymer Light-Emitting Diodes Using Graphene Oxide as a Hole Transport Layer. ACS Nano. 2012;6(4):2984-2991.
5. Weng Z, Dixon SC, Lee LY, Humphreys CJ, Guiney I, Fenwick O, et al. Wafer-Scale Graphene Anodes Replace Indium Tin Oxide in Organic Light-Emitting Diodes. Advanced Optical Materials. 2021;10(3).
6. Ma L-P, Wu Z, Yan Y, Zhang D, Dong S, Du J, et al. Stably doped graphene transparent electrode with improved light-extraction for efficient flexible organic light-emitting diodes. Nano Research. 2023;16(11):12788-12793.
7. Wang T, Jing L-C, Zhu Q, Sagadevan Ethiraj A, Tian Y, Zhao H, et al. Fabrication of architectural structured polydopamine-functionalized reduced graphene oxide/carbon nanotube/PEDOT:PSS nanocomposites as flexible transparent electrodes for OLEDs. Appl Surf Sci. 2020;500:143997.
8. Wang T, Wang Y-Z, Jing L-C, Zhu Q, Ethiraj AS, Geng W, et al. Novel biodegradable and ultra-flexible transparent conductive film for green light OLED devices. Carbon. 2021;172:379-389.
9. Tian Y, Wang T, Zhu Q, Zhang X, Ethiraj AS, Geng W-M, et al. High-Performance Transparent PEDOT: PSS/CNT Films for OLEDs. Nanomaterials. 2021;11(8):2067.
10. Valentini C, Montes-García V, Livio PA, Chudziak T, Raya J, Ciesielski A, et al. Tuning the electrical properties of graphene oxide through low-temperature thermal annealing. Nanoscale. 2023;15(12):5743-5755.
11. Wu J, Lin H, Moss DJ, Loh KP, Jia B. Graphene oxide for photonics, electronics and optoelectronics. Nature Reviews Chemistry. 2023;7(3):162-183.
12. Fu X, Lin J, Liang Z, Yao R, Wu W, Fang Z, et al. Graphene oxide as a promising nanofiller for polymer composite. Surfaces and Interfaces. 2023;37:102747.
13. Rathi V, Singh K, Parmar KPS, Brajpuriya RK, Kumar A. Improved thermoelectric performance of PEDOT:PSS/Bi_2Te_3/reduced graphene oxide ternary composite films for energy harvesting applications. RSC Advances. 2024;14(47):34883-34892.
14. Chen S, Cao W, Liu T, Tsang S-W, Yang Y, Yan X, et al. On the degradation mechanisms of quantum-dot light-emitting diodes. Nature Communications. 2019;10(1).
15. Moon H, Lee C, Lee W, Kim J, Chae H. Stability of Quantum Dots, Quantum Dot Films, and Quantum Dot Light-Emitting Diodes for Display Applications. Adv Mater. 2019;31(34).
16. Jang E, Jang H. Review: Quantum Dot Light-Emitting Diodes. Chem Rev. 2023;123(8):4663-4692.
17. Cho K-S, Lee EK, Joo W-J, Jang E, Kim T-H, Lee SJ, et al. High-performance crosslinked colloidal quantum-dot light-emitting diodes. Nature Photonics. 2009;3(6):341-345.
18. Li M, Li R, Wu L, Lin X, Xia X, Ao Z, et al. Ultrabright and stable top-emitting quantum-dot light-emitting diodes with negligible angular color shift. Nature Communications. 2024;15(1).
19. Lee T, Kim BJ, Lee H, Hahm D, Bae WK, Lim J, et al. Bright and Stable Quantum Dot Light-Emitting Diodes. Adv Mater. 2021;34(4).
20. Wang L, Lin J, Hu Y, Guo X, Lv Y, Tang Z, et al. Blue Quantum Dot Light-Emitting Diodes with High Electroluminescent Efficiency. ACS Applied Materials and Interfaces. 2017;9(44):38755-38760.
21. Li D, Bai J, Zhang T, Chang C, Jin X, Huang Z, et al. Blue quantum dot light-emitting diodes with high luminance by improving the charge transfer balance. Chem Commun. 2019;55(24):3501-3504.
22. Shi Y-L, Liang F, Hu Y, Wang X-D, Wang Z-K, Liao L-S. High-efficiency quantum dot light-emitting diodes employing lithium salt doped poly(9-vinlycarbazole) as a hole-transporting layer. Journal of Materials Chemistry C. 2017;5(22):5372-5377.
23. Kim DH, Hwang JH, Seo E, Lee K, Lim J, Lee D. Solution-Processed Thick Hole-Transport Layer for Reliable Quantum-Dot Light-Emitting Diodes Based on an Alternatingly Doped Structure. ACS Applied Materials and Interfaces. 2024;16(34):45139-45146.
24. He H, Ai Y, Shen P, Wang Z, Zhang H, Zhou Y, et al. Enhanced performance of perovskite light-emitting diodes with PEDOT:PSS/CsBr composite hole transport layer. Opt Mater. 2024;153:115638.